Structure-compressibility relationships in layered cuprate materials

Neil C. Hyatt,* Joseph A. Hriljac,† Yuzuru Miyazaki,‡ Ian Gameson, and Peter P. Edwards
School of Chemistry, University of Birmingham, Edgbaston, Birmingham B15 2TT, United Kingdom

Andrew P. Jephcoat
Department of Earth Sciences, University of Oxford, Parks Road, Oxford OX1 3PR, United Kingdom
(Received 7 July 2001; published 30 November 2001)

High-resolution synchrotron x-ray powder-diffraction experiments have been undertaken on the related series of layered cuprates of chemical formula $HgBa_2CuO_{4+\delta}$, $Hg_{0.8}Cr_{0.2}Ba_2CuO_{4+\delta}$, $Sr_2CuO_2CO_3$, $NbSr_2EuCu_2O_8$, $GaSr_2YCu_2O_7$, and $Pb_2Sr_2YCu_3O_{8+\delta}$ to applied pressures of 6.05, 7.64, 5.56, 4.47, 6.00, and 6.03 GPa, respectively. No discernible structural phase transitions were observed over these pressure ranges. The data have been analyzed using the Murnaghan formula to derive compressibilities and bulk moduli. The ambient pressure bulk moduli for the various cuprates are 63(2), 64(2), 62(2), 120(4), 85(3), and 129(4) GPa, respectively. In all cases the compressibility is the highest in the direction perpendicular to the cuprate layers (out-of-plane) and very anisotropic, with ratios for the out-of-plane to the in-plane compressibilities of 1.38, 1.25, 1.97, 1.45, 1.37 and 3.31, respectively. These variations are discussed in light of the crystal chemistry of these systems, and the observed trends should be helpful in tailoring the response of layered cuprates to applied hydrostatic pressure.

DOI: 10.1103/PhysRevB.65.014507 PACS number(s): 74.25.−q, 74.72.−h, 61.10.Nz, 64.30.+t

I. INTRODUCTION

The study of crystal structure-property relationships in layered cuprate superconductors is essential, since an understanding of the relationship between the electronic properties and crystal chemistry of these materials may guide future efforts toward the design and synthesis of cuprate materials with yet higher superconducting transition temperatures or improved properties. It is well known that the superconducting properties of cuprate materials may be precisely controlled by judicious manipulation of chemical stoichiometry. Indeed, it was exactly this strategy that allowed Bednorz and Müller to induce high-temperature superconductivity below 30 K in the antiferromagnetic insulator La_2CuO_4, by partial substitution of La by Ba.[1] Shortly after this discovery, Chu *et al*. reported the observation of superconductivity above 40 K in $La_{1.85}Ba_{0.15}CuO_4$, by compressing this material, with a T_c of 36 K at ambient pressure, to 1.3 GPa.[2] This impressive enhancement of T_c under pressure inspired Chu and co-workers to speculate that ''superconductivity at temperatures greatly exceeding 40 K is achievable in $La_{2-x}Ba_xCuO_4$ and related systems through fine tuning of the sample parameters through physical and chemical means.''[2] Stimulated by the work of Bednorz and Müller, and Chu and co-workers, the search for cuprate superconductors with improved superconducting properties has thus followed a dual strategy of controlling superconductivity through both methods of careful chemical substitution and application of high-pressure.

With the aim of discovering high-temperature superconductors with increased transition temperatures, high-pressure investigations have a significant advantage over methods of chemical substitution. In general, subtle and complex structural distortions may arise in a material of interest as a result of heterovalent or aliovalent chemical substitution. The resultant changes in physical properties induced by chemical substitution are, therefore, often difficult (if not impossible) to deconvolute from the effects of induced structural distortions. In contrast, the effect of applied hydrostatic pressure is only to compress interatomic separations and, consequently, changes in physical properties may be correlated *directly* with changes in interatomic bond lengths and bond angles. Studies of cuprate superconductors under high pressure, therefore, fulfil a unique role in furthering our understanding of these chemically and physically complex compounds, as reviewed by Wijngaarden and Griessen,[3] Schilling and Klotz,[4] Takahashi and Mori,[5] and Yamauchi and Karppinen.[6]

Hazen and Finger suggest that the compressibility of a solid material may be understood to be ''a function of polyhedral linkages and polyhedral bulk moduli.''[7] In accordance with this principle, the purpose of the present study was to establish the key structural features important in governing the compressibility of six layered copper oxide materials, namely, $HgBa_2CuO_{4+\delta}$, $Hg_{0.8}Cr_{0.2}Ba_2CuO_{4+\delta}$, $Sr_2CuO_2CO_3$, $NbSr_2EuCu_2O_8$, $GaSr_2YCu_2O_7$, and $Pb_2Sr_2YCu_3O_{8+\delta}$. The structures of these materials are illustrated schematically in Fig. 1. High-pressure powder x-ray diffraction studies were undertaken in order to determine the accurate compressibility parameters for these materials.

The crystal structure of $HgBa_2CuO_{4+\delta}$, Fig. 1(a), is tetragonal (space group $P4/mmm$) with unit-cell parameters of $a=3.877\,66(4)$ Å and $c=9.5073(1)$ Å at ambient pressure.[8] Partial random substitution of linear HgO_2^{2-} dumbbells in this compound by tetrahedral CrO_4^{2-} species affords the related compound $Hg_{0.8}Cr_{0.2}Ba_2CuO_{4+\delta}$, Fig. 1(b). The structure remains tetragonal, with unit-cell parameters of $a=3.9112(1)$ Å and $c=9.3458(3)$ Å at ambient pressure.[9] Although several groups have investigated pressure-induced structural changes in $HgBa_2CuO_{4+\delta}$, published estimates of the compressibility parameters of this compound differ widely, as discussed later. Thus, it was the first aim of the

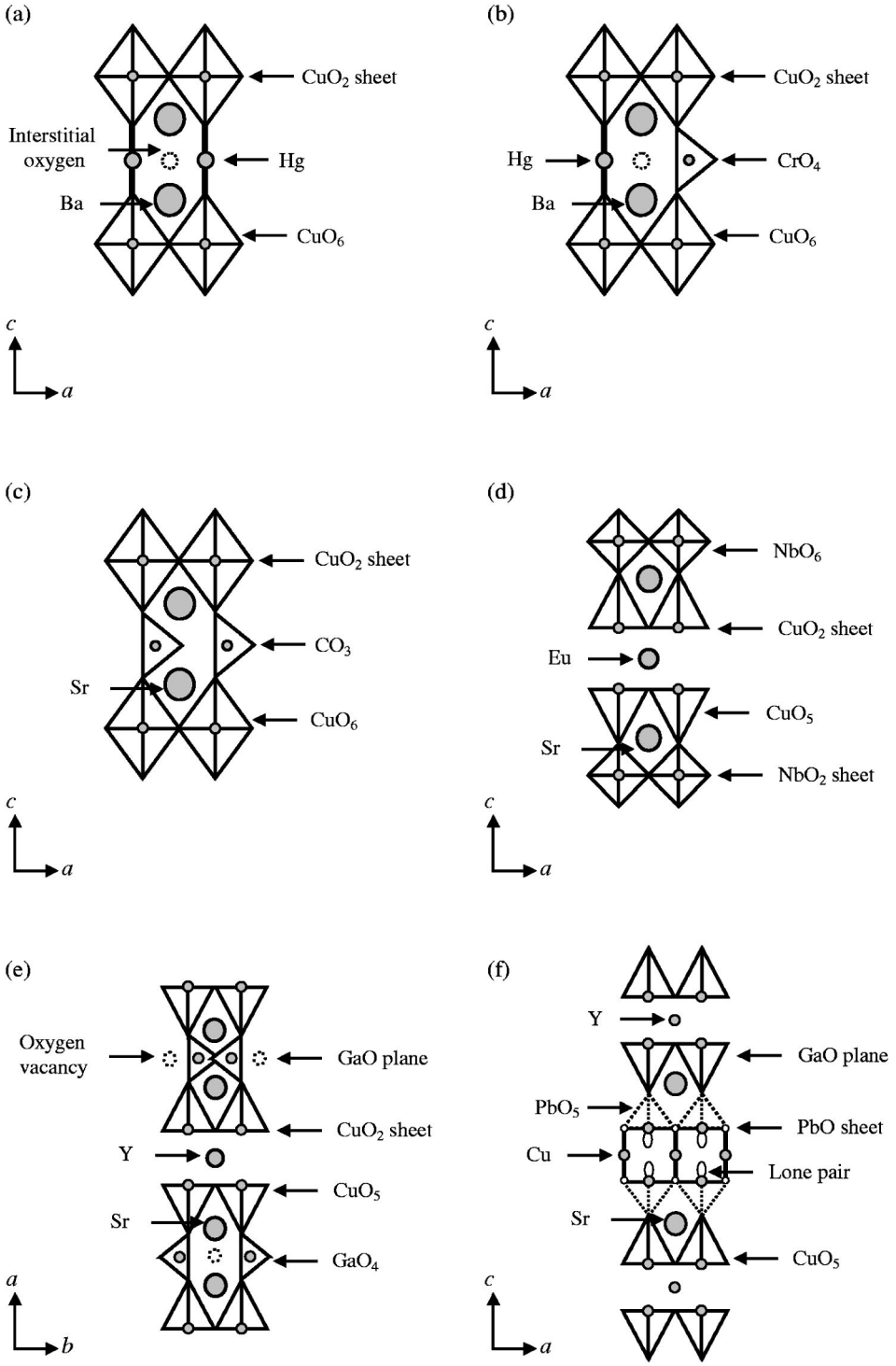

FIG. 1. Schematic representations of the crystal structures of (a) $HgBa_2CuO_{4+\delta}$, (b) $Hg_{0.8}Cr_{0.2}Ba_2CuO_{4+\delta}$, (c) $Sr_2CuO_2CO_3$, (d) $NbSr_2EuCu_2O_8$, (e) $GaSr_2YCu_2O_7$ and (f) $Pb_2Sr_2YCu_3O_{8+\delta}$.

present study to establish accurate compressibility parameters for $HgBa_2CuO_{4+\delta}$ and to assess the effect on these of partial substitution of chromium for mercury. The crystal structure of $Sr_2CuO_2CO_3$, Fig. 1(c), is clearly related to that of $HgBa_2CuO_{4+\delta}$ and consists of infinite layers of corner-sharing CuO_6 octahedra, connected by CO_3^{2-} carbonate units. This compound was first reported by Antipov and co-workers,[10] and then the details of its crystal structure were given by Miyazaki *et al.*[11] $Sr_2CuO_2CO_3$ crystallizes in the space group $I\bar{4}$, with unit-cell parameters $a=7.805(1)$ Å and $c=14.4993(1)$ Å at ambient pressure.[11] The compressibility of $Sr_2CuO_2CO_3$ was studied in order to compare it to that of $HgBa_2CuO_{4+\delta}$, and assess the effect of complete substitution of triangular CO_3^{2-} units for linear HgO_2^{2-} units.

The crystal structure of $NbSr_2EuCu_2O_8$, Fig. 1(d), may be considered as being composed of alternating oxygen-deficient perovskite-type $(CuO_2)(Eu)(CuO_2)$ layers and perovskite-type $(SrO)(NbO_2)(SrO)$ layers. This compound, first reported by Greaves and Slater, crystallizes in the space group $P4/mmm$, with unit-cell parameters $a=3.8733(1)$ Å

and $c=11.6322(4)$ Å, at ambient pressure.[12] The crystal structure of $GaSr_2YCu_2O_7$ is closely related to that of $NbSr_2EuCu_2O_8$, and may be considered as being composed of alternating oxygen-deficient perovskite-type $(CuO_2)(Y)(CuO_2)$ layers and oxygen-deficient perovskite type (SrO)(GaO)(SrO) layers, as shown in Fig. 1(e).[13] The oxygen vacancies in the (SrO)(GaO)(SrO) perovskite-type unit are ordered such that one-sixth of the anions normally present in the ABO_3 perovskite structure (where *A* represents a large 12-co-ordinate cation and *B* represents a small 6-co-ordinate cation) are removed from alternate [110] rows of each BO_2 plane. A small shift of the *B* cations in the anion-deficient layers allows these ions (Ga) to adopt tetrahedral co-ordination. The ordered nature of the oxygen vacancies and shift of the gallium cations, in the anion-deficient perovskite layer, results in an orthorhombic structure with unit-cell parameters related to the cubic perovskite unit-cell parameter, a_p, by $a\sim\sqrt{2}a_p$, $b\sim\sqrt{2}a_p$, and $c\sim 4a_p$. $GaSr_2YCu_2O_7$ was first reported by Roth *et al.*,[13] and crystallizes in the space group *Ima*2, with unit-cell parameters $a=22.801(5)$ Å, $b=5.4819(1)$ Å, and $c=5.3936(1)$ Å, at ambient pressure (note that the CuO_2 sheets are co-planar with the b,c plane in this material). High-pressure diffraction studies of $NbSr_2EuCu_2O_8$ and $GaSr_2YCu_2O_7$ were undertaken in order to compare the compressibility of these two compounds in the context of their close structural relationship.

The crystal structure of $Pb_2Sr_2YCu_3O_{8+\delta}$ $(\delta\sim 0)$ may be considered as being composed of alternating oxygen-deficient perovskite-type $(CuO_2)(Y)(CuO_2)$ layers and oxygen-deficient double rock-salt-type $(SrO)(PbO)(CuO_\delta)(PbO)(SrO)$ layers, as shown schematically in Fig. 1(f). This compound was first reported by Cava *et al.* and it crystallizes in the space group *Cmmm*, with unit-cell parameters $a=5.3933(1)$ Å, $b=5.4311(1)$ Å, and $c=15.7334(3)$ Å, at ambient pressure.[14] The orthorhombic symmetry of $Pb_2Sr_2YCu_3O_{8+\delta}$ arises from disorder in the PbO layers as a result of the stereoactive lone pairs of the Pb^{2+} ions, which cause static displacements of the neighboring oxygen atoms in the basal planes of the PbO_5 pyramids. The crystal structure of $Pb_2Sr_2YCu_3O_{8+\delta}$ thus contains infinite CuO_2 sheets formed from corner-sharing CuO_5 pyramids and infinite PbO sheets formed from edge-sharing PbO_5 pyramids. The in-plane compressibility of $Pb_2Sr_2YCu_3O_{8+\delta}$ might be expected to be rather small, due to cation-cation repulsions in the PbO-layers. To investigate this hypothesis, a high-pressure diffraction study of $Pb_2Sr_2YCu_3O_{8+\delta}$ was undertaken.

II. EXPERIMENT

A. Sample preparation

Essentially single-phase samples of $HgBa_2CuO_{4+\delta}$, $Hg_{0.8}Cr_{0.2}Ba_2CuO_{4+\delta}$, $Sr_2CuO_2CO_3$, $NbSr_2EuCu_2O_8$, $GaSr_2YCu_2O_7$ and $Pb_2Sr_2YCu_3O_{8+\delta}$ were prepared according to the methods described below. The phase purity of each sample was assessed by laboratory powder x-ray diffraction using a Siemens D5000 diffractometer operating in transmission mode with a primary beam Ge-(220) monochromator (affording Cu $K_{\alpha 1}$ radiation) and a position sensitive detector.

Samples of $HgBa_2CuO_{4+\delta}$ and $Hg_{0.8}Cr_{0.2}Ba_2CuO_{4+\delta}$ were prepared, via a solid-state reaction, from stoichiometric quantities of HgO, Cr_2O_3, and $Ba_2CuO_{3+\delta}$ according to the procedure described by Hyatt *et al.*[15] Specimens of $Sr_2CuO_2CO_3$ were prepared from stoichiometric amounts of $SrCO_3$ and CuO, according to the method of Miyazaki *et al.*[11] Samples of $NbSr_2EuCu_2O_8$ and $GaSr_2YCu_2O_7$ were prepared from stoichiometric amounts of Nb_2O_5, Ga_2O_3, Eu_2O_3, Y_2O_3, $SrCO_3$, and CuO. These reagents were intimately mixed, heated to 1000 °C for 12 h under flowing oxygen gas, and furnace-cooled to room temperature. The product from this initial reaction step was thoroughly ground, heated to 1050 °C for 20 hr under flowing oxygen gas, and furnace cooled to room temperature. This process was repeated several times until essentially single-phase materials were obtained. The preparation of samples of $Pb_2Sr_2YCu_3O_{8+\delta}$ $(\delta\sim 0)$ was achieved by a different procedure, in which stoichiometric quantities of PbO, SrO_2, Y_2O_3, and CuO were intimately mixed, heated to 850 °C for 6 h under a flowing atmosphere of nitrogen (99%) and oxygen (1%) gases, and furnace cooled to room temperature. The product from this initial reaction step was thoroughly ground, heated to 800 °C for 12 h under a flowing atmosphere of nitrogen (99%) and oxygen (1%) gases, and furnace cooled to room temperature. This process was repeated several times until an essentially single-phase material was obtained.

B. High-pressure x-ray diffraction studies

High-pressure powder x-ray diffraction experiments were performed using a diamond anvil cell (DAC), at the second-axis position of the three-axis diffractometer on the bending-magnet beam-line X7A, at the National Synchrotron Light Source, Brookhaven National Laboratory. The primary white beam from the bending magnet is focused in the horizontal plane by a triangular, asymmetrically cut Si-(220) monochromator, similar to that described by Lemmonier *et al.*,[16] which is bent to cylindrical curvature by applying a load to the crystal tip, affording monochromatic radiation of ~0.7 Å. The detector is a gas-proportional position-sensitive detector (PSD), based on the design of Boie *et al.*[17] with an active area of 10×1 cm^2 operating in a gas mixture of 90% Kr and 10% CO_2 at 0.4 MPa. The detector is located at ~45 cm from the sample position at the second axis center, which provides the optimum trade-off between resolution and intensity. The PSD allows simultaneous collection of data over a 10° window of scattering angle, although in the present study only the central ±2° region was used to minimize parallax errors. The PSD was stepped in 0.25° intervals over the desired angular range (typically 2°–35° 2θ) with the collected data frames normalized to the incident-beam intensity and merged to give the final diffraction pattern. The wavelength of the incident beam, $\lambda=0.68570(4)$ Å, was accurately determined from a sample of CeO_2 ($a_o=5.4113$ Å) spread on adhesive Kapton tape and located at

the second axis center. The wavelength and PSD parameters (zero channel and degrees per channel) were obtained from a least-squares fit of the Bragg reflections of CeO_2.

Finely powdered samples of $HgBa_2CuO_{4+\delta}$, $Hg_{0.8}Cr_{0.2}Ba_2CuO_{4+\delta}$, $Sr_2CuO_2CO_3$, $NbSr_2EuCu_2O_8$, $GaSr_2YCu_2O_7$, and $Pb_2Sr_2YCu_3O_{8+\delta}$ were, in turn, loaded into the DAC at ambient pressure and room temperature with a few small ruby chips. The DAC is based on a modified Merrill-Bassett design,[18] and employs two opposed 0.32 carat diamonds, with 0.5 mm diameter culets, on tungsten-carbide supports. The incident x-ray beam is admitted by a 0.5 mm diameter aperture, and the exit beam leaves via a rectangular 0.5×3.0 mm^2 tapered slit, oriented perpendicular to the horizontal plane of the diffractometer when the DAC is in position. The sample chamber was provided by a 200 μm hole drilled in the center of a 300 μm thick Inconel gasket, preindented to a thickness of 100 μm. A mixture, 4:1 by volume, of methanol:ethanol [which is known to remain hydrostatic to $\sim$10 GPa (Ref. 19)] was used as a pressure transmission medium. The applied hydrostatic pressure was measured by detecting the shift in the $R1$ emission line of ruby chips, placed in the sample chamber, using standard techniques.[20]

Reflection positions were determined from the diffraction data by fitting pseudo-Voigt profiles to each reflection.[21] These accurate reflection positions were then used in a least-squares procedure to obtain unit-cell parameters.

C. Data analysis

At moderate pressures, the empirical Murnaghan equation of state (EOS), Eq. (1), may be employed to analyze experimental compressibility data,[22,23]

$$\frac{q}{q_0}=\left[\left(\frac{\kappa_{q_0}}{\kappa'_{q_0}}\right)p+1\right]^{-\kappa'_{q_0}}. \tag{1}$$

In Eq. (1), p denotes pressure, q represents the parameter under compression (i.e., a unit-cell parameter or unit-cell volume), κ_q denotes its compressibility, and κ'_q denotes the pressure dependence of κ_q. The subscript zero denotes the ambient pressure value of a given variable. The Murnaghan EOS assumes that the modulus of a parameter, the inverse of its compressibility, has a linear pressure dependence. So, for example, the isothermal bulk modulus B is defined at any pressure p via

$$B=B_0+B'_0p, \tag{2}$$

where B_0 is the ambient pressure bulk modulus and B'_0 the associated pressure derivative. A specific form of the Murnaghan EOS based on the bulk modulus is

$$p=\frac{B_0}{B'_0}\left[\left(\frac{V_0}{V}\right)^{B'_0}-1\right], \tag{3}$$

where V is the unit-cell volume at pressure p and V_0 is the unit-cell volume at ambient pressure. Equations (1) and (3) were fitted to the experimental data in the form of plots of q/q_0 against pressure, using a Levenberg-Mardquart algorithm,[24] with each data point weighted by the square of the associated standard deviation.

In accordance with convention, the compressibility data reported for each of the compounds studied comprises the linear unit-cell compressibilities (denoted κ_a, κ_b, and κ_c), the volume compressibility (denoted κ_V), and the bulk modulus (denoted B_0), together with the pressure derivatives of each of these quantities. As a consequence of their layered nature, cuprate superconductors commonly show highly anisotropic compressibility, with the compressibility in the plane of the CuO_2 sheets being much less than in the direction perpendicular to the CuO_2 sheets (the out-of-plane compressibility). A useful parameter for expressing this anisotropy is the ratio of the out-of-plane to in-plane compressibility, denoted γ_κ, as given by

$$\gamma_\kappa=\frac{\kappa_{op}}{\kappa_{ip}}, \tag{4}$$

where κ_{op} denotes the out-of-plane compressibility and κ_{ip} denotes the in-plane compressibility. For tetragonal structures $\kappa_{ip}=\kappa_a=\kappa_b$, whereas for orthorhombic structures $\kappa_{ip}\sim\frac{1}{2}(\kappa_a+\kappa_b)$, where a and b represent the unit-cell parameters bounding the CuO_2 sheets. A related parameter is the ratio of the out-of-plane to average in-plane unit-cell parameter at ambient pressure

$$\gamma_{lp}=\frac{c}{\frac{1}{2}(a+b)}. \tag{5}$$

III. RESULTS AND DISCUSSION

Powder x-ray diffraction patterns of $HgBa_2CuO_{4+\delta}$, $Hg_{0.8}Cr_{0.2}Ba_2CuO_{4+\delta}$, $Sr_2CuO_2CO_3$, $NbSr_2EuCu_2O_8$, $GaSr_2YCu_2O_7$, and $Pb_2Sr_2YCu_3O_{8+\delta}$ were successfully acquired between ambient pressure and 6.05, 7.64, 5.56, 4.47, 6.00, and 6.03 GPa, respectively, with no observed phase transitions. Details of the refined unit-cell parameters are listed in Tables I–VI. In all cases, the unit-cell parameters of the samples were found to return to their ambient pressure values following pressure release. For all of the materials, Eq. (1) or (3) was used to derive the compressibility or bulk modulus values listed in Table VII, respectively. Plots of the data are presented in Figs. 2–7, with the smooth lines representing the weighted nonlinear least-squares fit of the Murnaghan EOS to the data.

A. Compressibility of $HgBa_2CuO_{4+\delta}$, $Hg_{0.8}Cr_{0.2}Ba_2CuO_{4+\delta}$, $Sr_2CuO_2CO_3$

The high-pressure behavior of $HgBa_2CuO_{4+\delta}$ has been previously reported by several groups, using a range of diffraction techniques. However, as shown in Table VIII, published estimates of the compressibility of $HgBa_2CuO_{4+\delta}$ appear to differ widely. The EOS parameters determined in this study are found to be in excellent agreement with those determined by Eggert *et al.*[25] (within the estimated errors). In contrast, the EOS parameters of Kim *et al.*[26] are observed to

TABLE I. Refined unit-cell parameters and unit-cell volume of $HgBa_2CuO_{4+\delta}$ at various pressures.

Pressure (GPa)	*a* parameter (Å)	*c* parameter (Å)	Volume (Å^3)
0.00	3.8851(7)	9.526(2)	143.79(5)
0.23(1)	3.8817(7)	9.510(2)	143.29(5)
1.04(1)	3.8668(7)	9.464(2)	141.51(5)
1.94(1) [a]	3.8548(8)	9.414(3)	139.89(6)
3.31(1)	3.8738(7)	9.345(3)	137.64(6)
4.18(1) [a]	3.826(1)	9.295(4)	136.06(8)
4.49(1)	3.8232(9)	9.277(3)	135.60(6)
5.04(1) [a]	3.819(2)	9.273(3)	135.2(2)
6.05(1) [a]	3.810(3)	9.22(1)	133.9(2)

[a]Data acquired in a second compression cycle.

TABLE II. Refined unit-cell parameters and unit-cell volume of $Hg_{0.8}Cr_{0.2}Ba_2CuO_{4+\delta}$ at various pressures.

Pressure (GPa)	*a* parameter (Å)	*c* parameter (Å)	Volume (Å^3)
0.00	3.9063(7)	9.3330(2)	142.41(3)
2.33(1)	3.8667(7)	9.217(1)	137.81(4)
3.38(1) [a]	3.845(1)	9.162(3)	135.45(5)
3.78(1)	3.842(1)	9.156(3)	135.13(7)
4.84(1)	3.823(1)	9.103(3)	133.04(7)
5.56(1) [a]	3.816(1)	9.018(3)	132.24(7)
6.78(1) [a]	3.801(1)	9.049(3)	130.74(7)
7.64(1) [a]	3.782(1)	8.999(3)	128.72(7)

[a]Data acquired in a second compression cycle.

TABLE III. Refined unit-cell parameters and unit-cell volume of $Sr_2CuO_2CO_3$ at various pressures.

Pressure (GPa)	*a* parameter (Å)	*c* parameter (Å)	Volume (Å^3)
0.00	7.8080(4)	14.9970(7)	914.29(8)
0.70(1)	7.784(1)	14.914(2)	903.7(1)
1.65(1)	7.764(1)	14.845(3)	894.9(2)
2.77(1)	7.729(1)	14.761(3)	881.8(2)
4.09(1)	7.706(1)	14.675(3)	871.4(2)
5.56(1)	7.680(1)	14.579(3)	859.9(2)

TABLE IV. Refined unit-cell parameters and unit-cell volume of $NbSr_2EuCu_2O_8$ at various pressures.

Pressure (GPa)	*a* parameter (Å)	*c* parameter (Å)	Volume (Å^3)
0.00	3.8747(8)	11.632(2)	174.63(6)
0.91(1)	3.8675(7)	11.600(2)	173.51(5)
2.06(1)	3.8562(4)	11.551(1)	171.77(3)
3.20(1)	3.8478(6)	11.510(2)	170.41(5)
4.77(1)	3.8366(6)	11.458(2)	168.66(5)

TABLE V. Refined unit-cell parameters and unit-cell volume of $GaSr_2YCu_2O_7$ at various pressures.

Pressure (GPa)	*a* parameter (Å)	*b* parameter (Å)	*c* parameter (Å)	Volume (Å ^{3})
0.00	22.808(7)	5.484(1)	5.406(1)	676.2(3)
0.85(1)	22.724(7)	5.468(1)	5.390(1)	669.7(3)
2.42(1)	22.604(7)	5.441(1)	5.363(1)	659.6(3)
3.63(1)	22.532(7)	5.423(1)	5.343(1)	652.9(3)
5.02(1)	22.463(8)	5.403(2)	5.322(2)	646.0(4)
6.00(1)	22.421(8)	5.391(2)	5.308(2)	641.6(4)

differ significantly from those determined by us and also by Eggert *et al*. The energy-dispersive x-ray diffraction data of both Eggert *et al.* and Kim *et al.* were acquired on beam-line X17 at the NSLS, BNL. Eggert *et al.* used a weighted least-squares fit of the Murnaghan equation in their data analysis, similar to that described in Sec. II C. Kim *et al.* also fit the Murnaghan equation to their compressibility data, however, each data point did not appear to be weighted by its associated error. The inherent uncertainty in the unit-cell parameters determined at a higher pressure is significantly greater than the uncertainty in the unit-cell parameters determined at a low pressure, since at higher pressures sample strain effects combined with collapse of the gasket aperture conspire to reduce the overall signal-to-noise ratio. The EOS parameters determined by Kim *et al.* may therefore be subject to some uncertainty since equal weighting appears to be given to data points acquired at all pressures.

Table VIII also includes estimates of the unit-cell and volume compressibilities and bulk modulus from the high-pressure neutron-diffraction studies of $HgBa_2CuO_{4+\delta}$ (to 5.0 GPa). The compressibility of $HgBa_2CuO_{4+\delta}$ was estimated by Akensov *et al.*[27] from a least-squares fit of a linear EOS to their compressibility data. However, the accuracy of the compressibility parameters reported by Akensov *et al.* is somewhat questionable, since a linear EOS does not model the pressure dependence of the compressibility of the crystal structure, which is considered to be significant over the pressure range studied. The compressibility data reported by Hunter *et al.*,[28] on optimally doped samples of $HgBa_2CuO_{4+\delta}$, were acquired from a powder neutron-diffraction study to 0.6 GPa. Hunter *et al.* also used a least-squares fit of a linear EOS to their compressibility data to derive their compressibility parameters. However, in this case, the method of analysis is justified, since below 1 GPa the pressure dependence of the bulk modulus is rather small, and the compressibility parameters may be regarded as reliable estimates of the initial compressibility of $HgBa_2CuO_{4+\delta}$. Balagurov *et al.* studied the compressibility of underdoped and overdoped samples of $HgBa_2CuO_{4+\delta}$ to 0.7 GPa, by powder neutron diffraction.[29] These authors also employ a least-squares fit of a linear equation in their data analysis. The difference between the initial compressibility parameters determined by Balagurov *et al.* and Hunter *et al.* was attributed, by Balagurov *et al.*, to the different oxygen contents of the samples under study.[29]

We note that our derived value for B_0' is somewhat larger than might be expected. Fits to the data using either the Birch or Vinet EOS (Ref. 23) gave essentially identical values for B_0 and B_0'. This confirms the validity of using the simpler Murnaghan EOS over the pressure range in this study, as has been found previously by others.[23,25]

The compressibility parameters of $Hg_{0.8}Cr_{0.2}Ba_2CuO_{4+\delta}$ and $HgBa_2CuO_{4+\delta}$ are very similar, and this, naturally, is considered to be a reflection of the close structural relationship between these two materials. It would appear that partial substitution of chromium for mercury has no significant effect on the overall compressibility of $HgBa_2CuO_{4+\delta}$. This is reasonable, since the majority of the common metal-oxide bonds in $HgBa_2CuO_{4+\delta}$ and $Hg_{0.8}Cr_{0.2}Ba_2CuO_{4+\delta}$ are of similar length, and may, therefore, be expected to be of similar compressibility. The compressibility of $Hg_{0.8}Cr_{0.2}Ba_2CuO_{4+\delta}$ is observed to be slightly less anisotropic than that of $HgBa_2CuO_{4+\delta}$. This, undoubtedly, is a reflection of the slightly reduced structural anisotropy of $Hg_{0.8}Cr_{0.2}Ba_2CuO_{4+\delta}$, with respect to that of $HgBa_2CuO_{4+\delta}$, as quantified by γ_{lp} in Table VII.

It is interesting to note that the bulk moduli of $Sr_2CuO_2CO_3$ and of $HgBa_2CuO_{4+\delta}$ are very similar, which may be a reflection of the close structural relationship between compounds. One might expect the bulk modulus of $Sr_2CuO_2CO_3$ to be significantly larger than that of $HgBa_2CuO_{4+\delta}$, since the mean Sr-O bond length (2.672 Å (Ref. 11) in the former compound is much shorter than the

TABLE VI. Refined unit-cell parameters and unit-cell volume of $Pb_2Sr_2YCu_3O_{8+\delta}$ at various pressures.

Pressure (GPa)	*a* parameter (Å)	*b* parameter (Å)	*c* parameter (Å)	Volume (Å ^{3})
0.00	5.389(1)	5.428(1)	15.712(3)	459.6(1)
0.86(1)	5.383(1)	5.421(1)	15.652(3)	456.7(1)
2.33(1)	5.373(1)	5.409(1)	15.562(3)	452.3(1)
4.13(1)	5.363(1)	5.396(1)	15.430(3)	446.6(1)
6.03(1)	5.353(1)	5.383(1)	15.351(3)	442.4(1)

TABLE VII. Summary of compressibility data for (a) $HgBa_2CuO_{4+\delta}$, (b) $Hg_{0.8}Cr_{0.2}Ba_2CuO_{4+\delta}$, (c) $Sr_2CuO_2CO_3$, (d) $NbSr_2EuCu_2O_8$, (e) $GaSr_2YCu_2O_7$, and (f) $Pb_2Sr_2YCu_3O_{8+\delta}$. γ_κ denotes the ratio of the out-of-plane to in-plane compressibility, γ_{lp} denotes the ratio of the out-of-plane to in-plane unit-cell parameters at ambient pressure.

Parameter	a	b	c	d	e	f
κ_{a_0} ($\times 10^{-3}$ GPa^{-1})	4.7(2)	4.7(3)	4.3(3)	2.4(4)	4.8(4)	1.3(2)
κ'_{a_0}	0.03(1)	0.12(7)	0.02(1)	0.03(3)	0.017(3)	0.02(1)
κ_{b_0} ($\times 10^{-3}$ GPa^{-1})					3.7(2)	1.6(2)
κ'_{b_0}					0.03(1)	0.03(2)
κ_{c_0} ($\times 10^{-3}$ GPa^{-1})	6.5(2)	5.9(4)	8.5(4)	3.5(1)	3.3(2)	4.8(2)
κ'_{c_0}	0.11(5)	0.08(3)	0.03(2)	0.08(2)	0.03(1)	0.06(1)
κ_{V_0} ($\times 10^{-3}$ GPa^{-1})	15.8(4)	15.4(6)	16.16(6)	8.3(3)	11.8(5)	7.7(3)
κ'_{c_0}	0.14(2)	0.28(7)	0.08(1)	0.14(1)	0.06(1)	0.10(3)
B_0 (GPa)	63(2)	64(2)	62(2)	120(4)	85(3)	129(4)
B'_0	7(1)	3(1)	12(2)	7(2)	15(2)	9(2)
γ_κ	1.38	1.25	1.97	1.45	1.37	3.31
γ_{lp}	2.45	2.39	1.86	3.00	2.96	4.11

mean Ba-O bond length (2.805 Å, Ref. 15) in the latter material. Clearly this is not the case. The crystal structure of $Sr_2CuO_2CO_3$ is significantly distorted with respect to that of $HgBa_2CuO_{4+\delta}$ due to the static displacement of the apical oxygen atoms bonded to the carbonate groups, see Fig. 5 of Ref. 11. Consequently, the SrO_9 and CuO_6 co-ordination polyhedra in $Sr_2CuO_2CO_3$ are considerably distorted from ideal geometry. The compression of $Sr_2CuO_2CO_3$ could, therefore, be accommodated, structurally, by further deformation of the SrO_9 and CuO_6 co-ordination polyhedra through a combination of compression and torsion of metal-oxide bond lengths and bond angles, respectively. This may account for the higher than expected compressibility of $Sr_2CuO_2CO_3$.

B. Compressibility of $NbSr_2EuCu_2O_8$ and $GaSr_2YCu_2O_7$

Although $NbSr_2EuCu_2O_8$ and $GaSr_2YCu_2O_7$ are closely related in structural terms, Fig. 1, the bulk modulus of $GaSr_2YCu_2O_7$ is much less than that of $NbSr_2EuCu_2O_8$. This may be attributable to the effect of ordered oxygen vacancies in the (SrO)(GaO)(SrO) perovskite-type layer connecting adjacent oxygen-deficient perovskite-type $(CuO_2)(Y)(CuO_2)$ layers in this material. These oxygen vacancies have the effect of breaking up the polyhedral connectivity in the connecting perovskite-type layer, leading to a significant increase in the in-plane compressibility of $GaSr_2YCu_2O_7$, mean value of 3.5×10^{-3} GPa^{-1}, with respect to that of $NbSr_2EuCu_2O_8$, 2.4×10^{-3} GPa^{-1}. The effect of oxygen vacancies on the relative compressibility of $YBa_2Cu_3O_{6.99}$ and $YBa_2Cu_3O_{6.60}$ has been interpreted using similar arguments. The initial compressibility of these compounds was determined by Jorgensen *et al.* from high-pressure neutron-diffraction studies to 0.6 GPa.[30] The effect of removing the chain-site oxygen in this compound is, most significantly, to increase the *b*-axis compressibility, as a result of breaking up the CuO chains that run parallel to the *b* axis in this compound. This, combined with a small increase in the unit-cell volume, leads to a reduced bulk modulus of 112 GPa in $YBa_2Cu_3O_{6.60}$ with respect to the bulk modulus of $YBa_2Cu_3O_{6.99}$ determined as 125 GPa.[30]

The compressibility in the *b* direction of $GaSr_2YCu_2O_7$ is found to be slightly greater than that in the *c* direction. In the structure of this compound the GaO_4 tetrahedra are corner linked to form infinite GaO chains, running parallel to the *c* direction in the *b*,*c*-plane. It would, therefore, appear that the GaO_4 chains make an additional contribution to the *c*-axis stiffness of $GaSr_2YCu_2O_7$, leading to a slightly smaller *c*-axis compressibility, with respect to the *b*-axis compressibility. A direct consequence of the slightly smaller compressibility of the *c* axis compared to that of the *b* axis in this compound is a decrease in the orthorhombic distortion with increasing pressure. The orthorhombicity parameter *e* can be defined by

$$e=\left|\frac{(x_1-x_2)}{(x_1+x_2)}\right|, \tag{6}$$

where x_1 and x_2 represent values of the orthorhombic unit-cell parameters (in this case the *b* and *c* parameters). The derived values of *e* are plotted in Fig. 8(a), along with the results of a weighted nonlinear least-squares fit of a second-order polynomial

$$e=e_0+e_1p+e_2p^2 \tag{7}$$

to the experimental data, obtained using the Levenberg-Mardquart algorithm. The refined values of e_0, e_1, and e_2 are 0.008 36(1), $-1.72(5)\times10^{-4}$ GPa^{-1} and $1.15(8)\times10^{-5}$ GPa^{-2}, respectively. As shown in Fig. 8(a), the orthorhombic distortion of $GaSr_2YCu_2O_7$ decreases with increasing pressure, although the change over the 6.00 GPa pressure range studied is rather small, $\sim$8%, suggesting that any possible pressure-induced orthorhombic-to-tetragonal phase transition should be expected at extremely high pressure. This expectation is supported by extrapolation of the pressure dependence of the *b*- and *c*-unit-cell parameters to

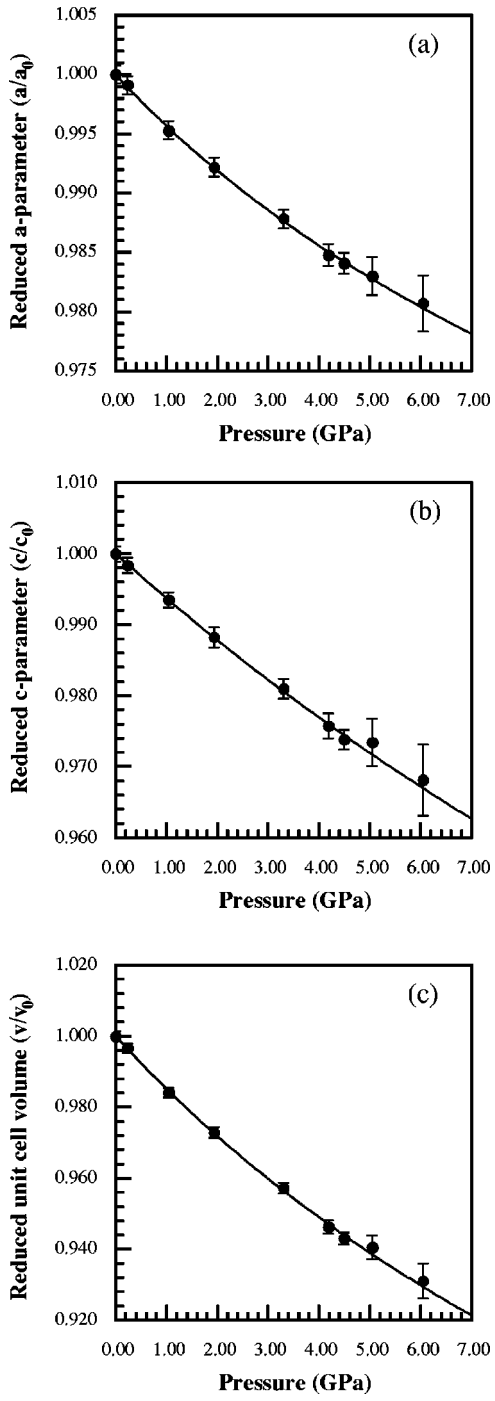

FIG. 2. Pressure dependence of (a) and (b) unit-cell parameters, and (c) unit-cell volume of $HgBa_2CuO_{4+\delta}$, normalized to their room-pressure values.

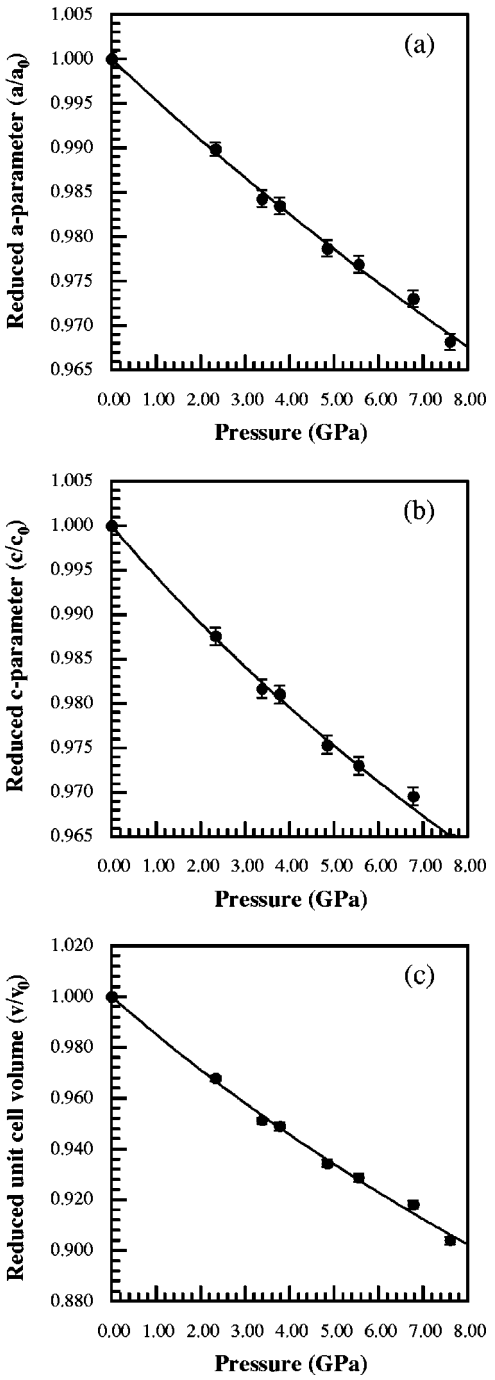

FIG. 3. Pressure dependence of (a) and (b) unit-cell parameters, and (c) unit-cell volume of $Hg_{0.8}Cr_{0.2}Ba_2CuO_{4+\delta}$, normalized to their room-pressure values

30 GPa (using the Murnaghan EOS parameters in Table VII), as shown in Fig. 8(b). This extrapolation indicates that such an orthorhombic-to-tetragonal phase transition should be expected at pressures well in excess of 30 GPa.

C. Compressibility of $Pb_2Sr_2YCu_3O_{8+\delta}$

The pressure dependence of the orthorhombicity parameter e for $Pb_2Sr_2YCu_3O_{8+\delta}$ is shown in Fig. 9(a), where the variables x_1 and x_2 in Eq. (6) represent values of the *a*- and *b*-unit-cell parameters. The smooth line represents a weighted nonlinear least-squares fit to the data of a second-order polynomial defined by Eq. (7), obtained using the Levenberg-Mardquart algorithm. The refined values of e_0, e_1, and e_2 are 0.003 60(1), $-1.4(1)\times10^{-4}$ GPa^{-1} and $5.1(2)\times10^{-7}$ GPa^{-2}, respectively. As shown in Fig. 9(a), the orthorhombic distortion of $Pb_2Sr_2YCu_3O_{8+\delta}$ decreases with increasing pressure. The change in the orthorhombicity

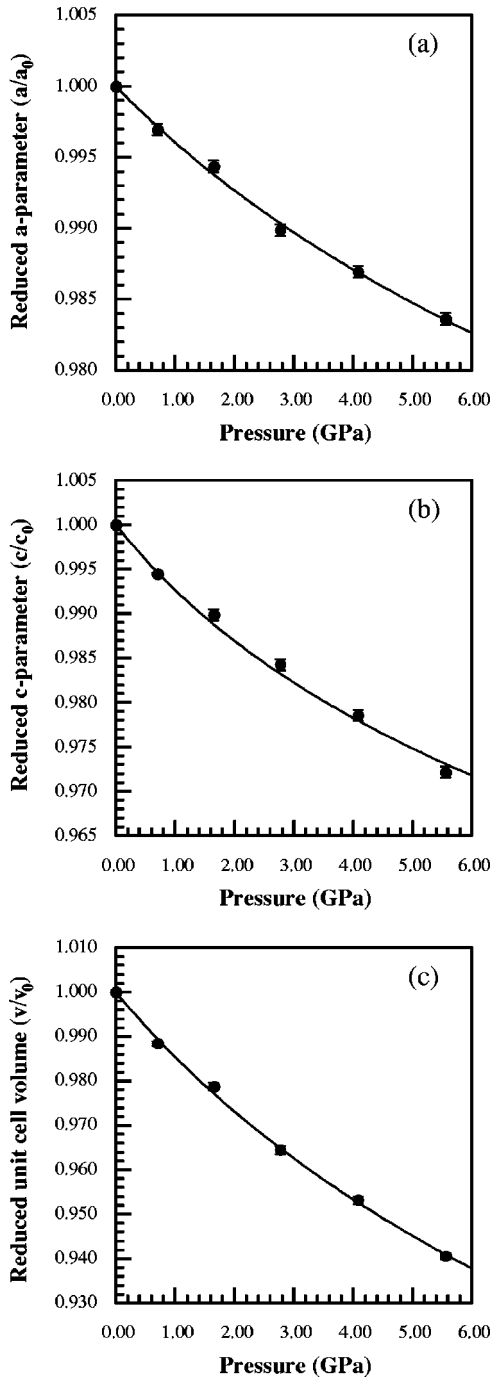

FIG. 4. Pressure dependence of (a) and (b) unit-cell parameters, and (c) unit-cell volume of $Sr_2CuO_2CO_3$, normalized to their room-pressure values.

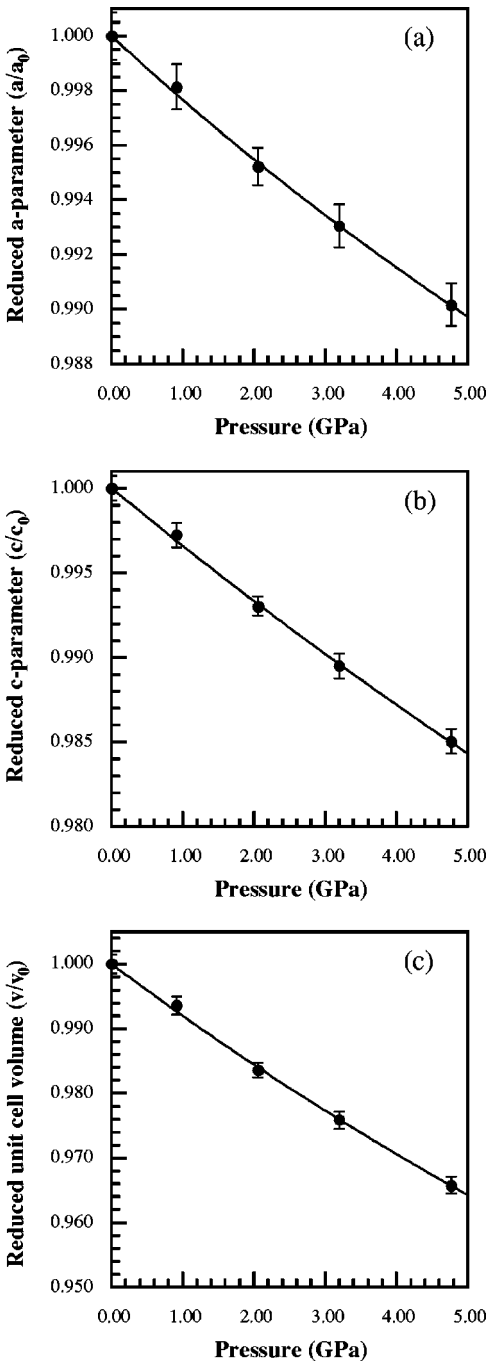

FIG. 5. Pressure dependence of (a) and (b) unit-cell parameters, and (c) unit-cell volume of $NbSr_2EuCu_2O_8$, normalized to their room-pressure values.

parameter of $Pb_2Sr_2YCu_3O_{8+\delta}$ over the 6.0 GPa pressure range studied is rather large, ~25%, suggesting that a pressure-induced orthorhombic-to-tetragonal phase transition should be expected at moderately higher pressures. This expectation is supported by extrapolation of the pressure dependence of the *a*- and *b*-unit-cell parameters to 30 GPa using the Murnaghan EOS parameters in Table VII, Fig. 9(b). This extrapolation suggests that an orthorhombic-to-tetragonal phase transition may occur in the region of ~30 GPa. The orthorhombic distortion of $Pb_2Sr_2YCu_3O_{8+\delta}$ arises from the subtle displacements of the oxygen atoms in the PbO layers of this material, induced by the stereoactive lone pairs of the Pb^{2+} cations. It is difficult to comment further on the relative compressibility of the *a* and *b* axes of this compound in the absence of a model describing the precise structure of the PbO layers in this material. However, it is reasonable to note that the slightly larger compressibility of the *b* axis with respect to the *a* axis is consistent with the fact that the *b* axis is slightly longer than the *a* axis at ambient pressure.

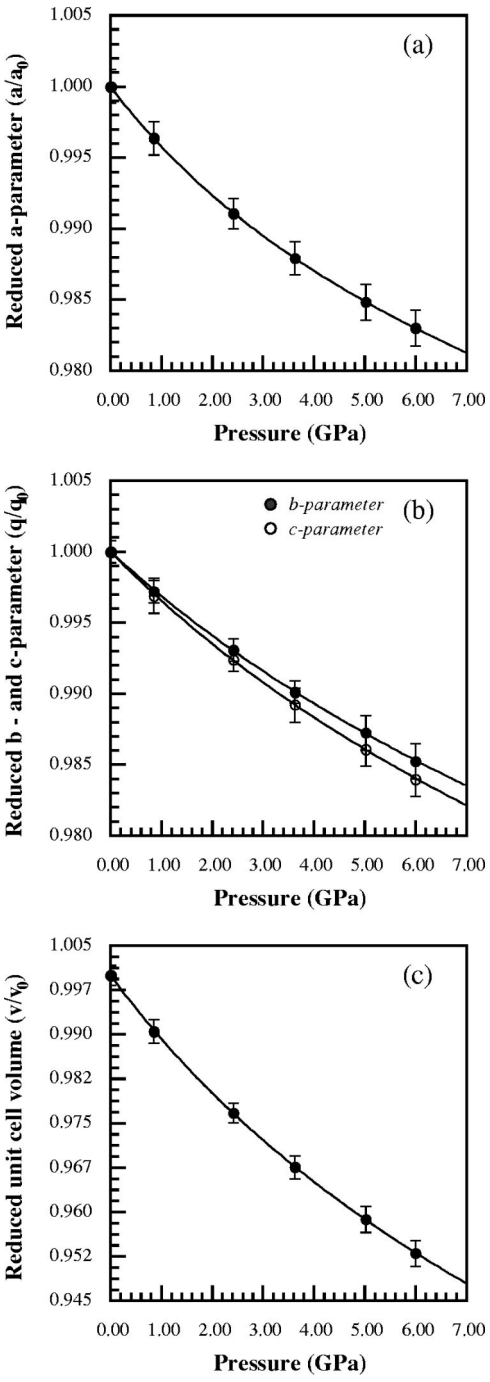

FIG. 6. Pressure dependence of (a) and (b) unit-cell parameters, and (c) unit-cell volume of $GaSr_2YCu_2O_7$, normalized to their room-pressure values.

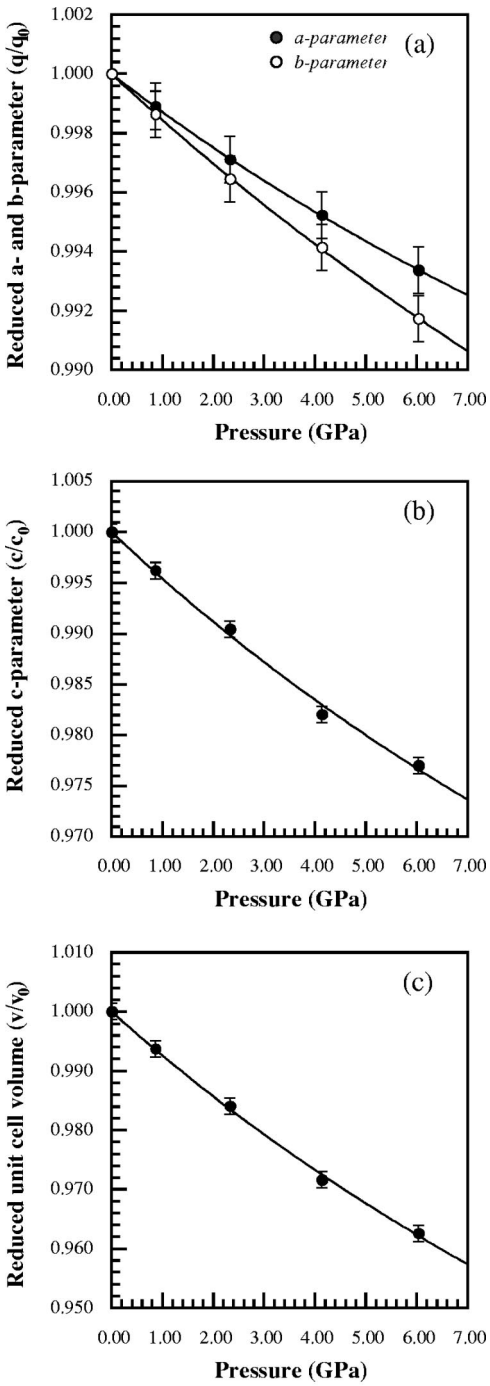

FIG. 7. Pressure dependence of (a) and (b) unit-cell parameters, and (c) unit-cell volume of $Pb_2Sr_2YCu_3O_{8+\delta}$, normalized to their room-pressure values.

A previous high-pressure x-ray diffraction study of $Pb_2Sr_2YCu_3O_{8+\delta}$ and $Pb_2Sr_2HoCu_3O_{8+\delta}$ was undertaken by Jorgensen *et al.* using energy-dispersive techniques.[31] Interestingly, they report an orthorhombic-to-tetragonal phase transition in $Pb_2Sr_2YCu_3O_{8+\delta}$ above ~10 GPa. However, this observation is subject to some uncertainty, as the authors themselves note, due to the limited resolution of that experiment. In our higher-resolution angle-dispersive x-ray diffraction study, the (020) and (220) reflections are well resolved at 6.03 GPa; this is in contrast with the energy-dispersive study in which these reflections could not be resolved, even at ambient pressure. As discussed earlier, the EOS parameters determined in this study support the possibility of a pressure-induced orthorhombic-to-tetragonal phase transition in $Pb_2Sr_2YCu_3O_{8+\delta}$, although at a significantly higher pressure than that proposed by Jorgensen *et al.*

The compressibility parameters reported by Jorgensen *et al.* are compared with those determined in this work in

TABLE VIII. EOS parameters for $HgBa_2CuO_{4+\delta}$ from various authors.

EOS Parameter	This work [a]	Eggert [a] Ref. 25	Kim [a] Ref. 26	Akensov [a] Ref. 27	Hunter [a] Ref. 28	Balagurov [b] Ref. 29	Balagurov [c] Ref. 29
κ_{a_0} ($\times 10^{-3}$ GPa^{-1})	4.7(2)	4.9(3)	2.05(1)	3.3(2)	4.26(5)	3.73(4)	3.60(6)
κ'_{a_0}	0.03(1)	0.04(1)	0.56				
κ_{c_0} ($\times 10^{-3}$ GPa^{-1})	6.5(2)	5.8(2)	7.46(4)	4.6(1)	5.83(9)	5.48(4)	4.90(6)
κ'_{c_0}	0.11(5)	0.20(4)	0.01				
κ_{V_0} ($\times 10^{-3}$ GPa^{-1})	15.8(4)	15.3(7)	9.62(5)	11.2(3)	14.3(1)	12.9(1)	12.1(2)
κ'_{V_0}	0.14(2)	0.22(2)	0.11				
B_0 (GPa)	63(2)	65(3)	104(6)	89(2)	69.9(5)	77.5(6)	69(1)
B'_0	7(1)	4.5(5)	8.61				

[a]Optimally doped.
[b]Underdoped.
[c]Overdoped.

Table IX, and it is apparent that most of the derived values differ substantially. We believe that these differences are due to the different experimental techniques and methods of data analysis employed in the two studies. The energy-dispersive data of Jorgensen *et al.* is of much lower resolution than our angle-dispersive data and, for the reasonably complicated orthorhombic crystal structure of $Pb_2Sr_2YCu_3O_{8+\delta}$, this may have led to significant inaccuracies in peak positions in the earlier study. The previous study also used a nonweighted nonlinear least-squares fit of the Murnaghan equation to the pressure-volume data to derive a bulk modulus, and a nonweighted second-order polynomial expression [similar to that of Eq. (7)] to evaluate the linear compressibilities. These methods are less reliable than those that we have employed, as discussed earlier for $HgBa_2CuO_{4+\delta}$. Given the inherently higher resolution of the present data and better methods of data analysis, we believe that the compressibility parameters of $Pb_2Sr_2YCu_3O_{8+\delta}$ that we have established are the most accurate to date.

D. General trends

The compressibilities of the layered cuprate materials studied in this work, summarized in Table VII, are generally observed to be anisotropic, as given by the ratio of out-of-plane to in-plane compressibilities, γ_κ, defined by Eq. (4). This is considered to arise from the Jahn-Teller distorted CuO_n ($n=5$ or 6) polyhedra, common to all these compounds, in which the apical Cu-O bond is found to be much longer than the in-plane Cu-O bond. As one might expect, the anisotropic compressibilities of these materials also appear to correlate with the inherent structural anisotropy of these compounds, quantified by the ratio of out-of-plane to in-plane unit-cell parameters at ambient pressure, denoted γ_{lp} in Table VII (assuming pseudotetragonal symmetry for $Pb_2Sr_2YCu_3O_{8+\delta}$ and $GaSr_2YCu_2O_7$, and normalizing the a parameter of $GaSr_2YCu_2O_7$ to account for the body centered symmetry of this structure). Thus, compounds with similar ratios of the out-of-plane to in-plane unit-cell parameters, for example, $HgBa_2CuO_{4+\delta}$ and $Hg_{0.8}Cr_{0.2}Ba_2CuO_{4+\delta}$, and $NbSr_2EuCu_2O_8$ and $GaSr_2YCu_2O_7$, are found to have similar ratios of out-of-plane to in-plane compressibilities.

A second overall trend to emerge from the data in Table VII is the general correlation of the in-plane compressibility with the number of layers formed by corner- and edge-shared metal-oxide polyhedra per unit interlayer distance (defined as the distance between adjacent CuO_2 sheets) in the crystal structure. $HgBa_2CuO_{4+\delta}$, $Hg_{0.8}Cr_{0.2}Ba_2CuO_{4+\delta}$, and $Sr_2CuO_2CO_3$, which have only one CuO_2 sheet per inter-

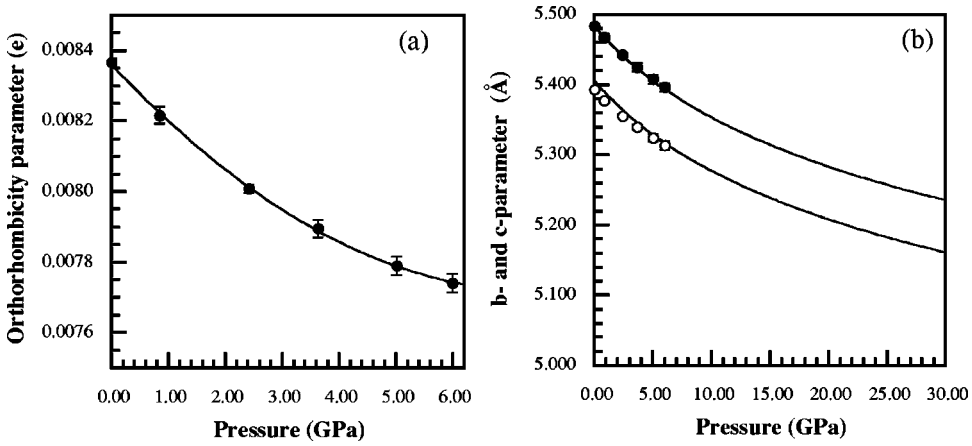

FIG. 8. (a) Pressure dependence of the orthorhombicity parameter of $GaSr_2YCu_2O_7$, and (b) extrapolated pressure dependence of the *b*- and *c*-unit-cell parameters using the Murnaghan EOS parameters in Table VII.

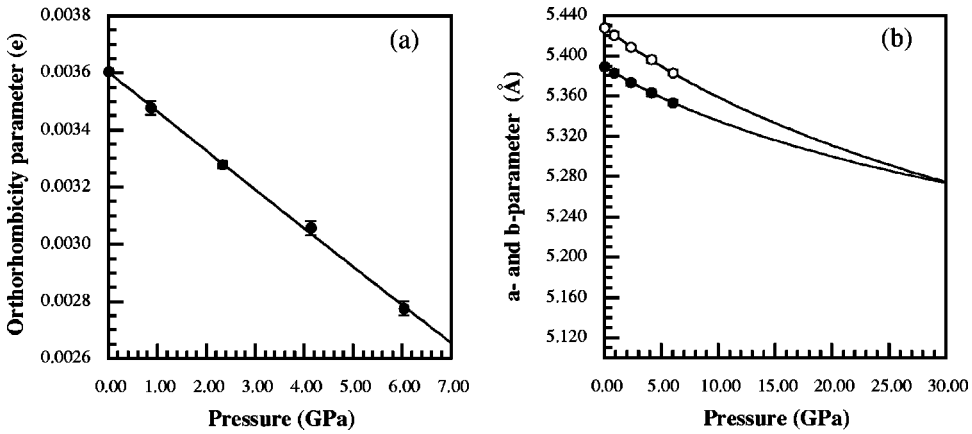

FIG. 9. (a) Pressure dependence of the orthorhombicity parameter of $Pb_2Sr_2YCu_3O_{8+\delta}$, and (b) extrapolated pressure dependence of the *a*- and *b*-unit-cell parameters using the Murnaghan EOS parameters in Table VII.

layer distance, all have an in-plane compressibility of $\kappa_{ip} \sim 4.5\times10^{-3}$ GPa^{-1}. $GaSr_2YCu_2O_7$ has two CuO_2 sheets per unit interlayer distance *plus* one oxygen deficient ''GaO''-plane, and has a lower in-plane compressibility of $\kappa_{ip} \sim 3.7\times10^{-3}$ GPa^{-1}. In comparison, $NbSr_2EuCu_2O_8$, which has two CuO_2 sheets *plus* one NbO_2 sheet per interlayer distance, has a smaller in-plane compressibility of $\kappa_{ip} = 2.4\times10^{-3}$ GPa^{-1}. The smallest in-plane compressibility, $\kappa_{ip} \sim 1.45\times10^{-3}$ GPa^{-1}, is found in $Pb_2Sr_2YCu_3O_{8+\delta}$, which has two CuO_2 sheets *plus* two PbO sheets (formed from edge-sharing PbO_5 pyramids) per interlayer distance. Thus, as one might anticipate, the in-plane compressibility decreases as the number of additional metal-oxide sheets per interlayer distance increases. The very high anisotropy of compressibility observed for $Pb_2Sr_2YCu_3O_{8+\delta}$, $\gamma_\kappa = 3.31$, results from the very low in-plane compressibility of this material. To the best of our knowledge, the compressibility of $Pb_2Sr_2YCu_3O_{8+\delta}$ is the most anisotropic of all high-temperature superconductors studied to date.

IV. SUMMARY

The compressibilities and bulk moduli of $HgBa_2CuO_{4+\delta}$, $Hg_{0.8}Cr_{0.2}Ba_2CuO_{4+\delta}$, $Sr_2CuO_2CO_3$, $NbSr_2EuCu_2O_8$, $GaSr_2YCu_2O_7$, and $Pb_2Sr_2YCu_3O_{8+\delta}$ have been determined from high-pressure powder x-ray diffraction experiments. Compressibility parameters for these materials have been established from fitting the Murnaghan EOS to the associated compressibility data. A number of general conclusions may be drawn, with regard to the compressibility of layered cuprate materials. In general, the anisotropic compressibility of a layered cuprate material is governed by the polyhedral connectivity of the crystal structure. In all cases, the compressibility in the direction perpendicular to the metal-oxide layers is greater than that in the plane of the layers due to the Jahn-Teller distortion in the CuO_n ($n=5$ or 6) polyhedra. Furthermore, the in-plane compressibility varies systematically with the number of metal-oxide sheets per unit interlayer distance, decreasing with an increasing number of metal-oxide sheets. Additionally, the in-plane compressibility appears to increase when the polyhedral connectivity in a given structural layer is disrupted. These trends may be important with a view to tailor the response of layered cuprates (and other materials in general) to applied pressure.

ACKNOWLEDGMENTS

The authors are grateful to Dr. David Cox and Dr. Tom Vogt (Brookhaven National Laboratory) for experimental assistance in the acquisition of high-pressure x-ray diffraction data. We acknowledge the Geophysical Lab of the Carnegie Institution of Washington for allowing us the use of the ruby laser system at beamline X17C for the pressure measure-

TABLE IX. Comparison of EOS parameters for $Pb_2Sr_2YCu_3O_{8+\delta}$ and $Pb_2Sr_2HoCu_3O_{8+\delta}$.

EOS Parameter	$Pb_2Sr_2YCu_3O_{8+\delta}$ This work	$Pb_2Sr_2YCu_3O_{8+\delta}$ Jorgensen (Ref. 31)	$Pb_2Sr_2HoCu_3O_{8+\delta}$ Jorgensen (Ref. 31)
κ_{a_0} ($\times10^{-3}$ GPa^{-1})	1.3(2)	1.8(3)	2.1(3)
κ'_{a_0}	0.02(1)		
κ_{b_0} ($\times10^{-3}$ GPa^{-1})	1.6(2)	2.0(3)	2.2(3)
κ'_{b_0}	0.03(2)		
κ_{c_0} ($\times10^{-3}$ GPa^{-1})	4.8(2)	1.8(3)	1.3(3)
κ'_{c_0}	0.06(1)		
κ_{V_0} ($\times10^{-3}$ GPa^{-1})	7.7(4)	6.3(4)	6.1(3)
κ'_{c_0}	0.10(3)	0.2	0.02(3)
B_0 (GPa)	129(4)	160(7)	164(5)
B'_0	9(2)	5.0	5.0(8)

ments, and the technical assistance of Dr. J. Z. Hu. We are also grateful to Dr. Ian Sims (School of Chemistry, University of Birmingham) for useful discussions concerning the mathematics of the Levenberg-Mardquardt algorithm. This research was carried out (in part) at the National Synchrotron Light Source, Brookhaven National Laboratory, which is supported by the U.S. Department of Energy, Division of Materials Sciences and Division of Chemical Sciences. We gratefully acknowledge the financial support of the Engineering and Physical Sciences Research Council and Merck Ltd.

*Present address: The London and Scandinavian Metallurgical Company Ltd., Fullerton Road, Rotherham, South Yorkshire, S60 1DL.

†Email address: j.a.hriljac@bham.ac.uk

‡Present address: Tohoku University, Graduate School of Engineering, Department of Applied Physics, Aoba Ku, Sendai, Miyagi 9808579, Japan.

[1] J. G. Bednorz and K. A. Müller, Z. Phys. B: Condens. Matter **64**, 189 (1986).

[2] C. W. Chu, P. H. Hor, R. L. Meng, L. Gao, Z. J. Huang, and Y. Q. Wang, Phys. Rev. Lett. **58**, 405 (1987).

[3] R. J. Wijngaarden and R. Griessen, in *Studies of High-temperature Superconductors*, edited by A. Narlikar (Nova Science, Huntington, NY, 1991), Vol. 2.

[4] J. S. Schilling and S. Klotz, in *Properties of High-Temperature Superconductors*, edited by D. M. Ginsberg (World Scientific, Singapore, 1992), Vol. 3.

[5] H. Takahashi and N. Mori, in *Studies of High-temperature Superconductors*, edited by A. Narlikar (Nova Science, Huntington, NY, 1996), Vol. 16.

[6] H. Yamauchi and M. Karpinnen, Supercond. Sci. Technol. **13**, 1233 (2000).

[7] R. M. Hazen and L. W. Finger, *Comparative Crystal Chemistry* (Wiley, New York, 1982).

[8] S. N. Putilin, E. V. Antipov, O. Chmaissem, and M. Marezio, Nature (London) **362**, 362 (1993).

[9] O. Chmaissem, J. D. Jorgensen, D. G. Hinks, B. G. Storey, B. Dabrowski, H. Zhang, and L. D. Marks, Physica C **279**, 1 (1997).

[10] D. V. Fomichev, A. L. Kharlanov, E. V. Antipov, and L. M. Kovba, Superconductivity: Physics, Chemistry, Engineering **3**, S126 (1990).

[11] Y. Miyazaki, H. Yamane, T. Kajitani, T. Oku, K. Hiraga, Y. Morii, K. Fuchizaki, S. Funahashi, and T. Hirai, Physica C **191**, 434 (1992).

[12] C. Greaves and P. R. Slater, IEEE Trans. Magn. **27**, 1174 (1991).

[13] G. Roth, P. Adelmann, G. Heger, R. Knitter, and Th. Wolf, J. Phys. I **1**, 721 (1991).

[14] R. J. Cava, B. Batlogg, J. J. Krajewski, L. W. Rupp, L. F. Schneemeyer, T. Siegrist, R. B. van Dover, P. Marsh, W. F. Peck, Jr., P. K. Gallagher, S. H. Glarum, J. H. Marshall, R. C. Farrow, J. V. Waszczak, R. Hull, and P. Trevor, Nature (London) **336**, 211 (1988).

[15] N. C. Hyatt, J. P. Hodges, I. Gameson, S. Hull, and P. P. Edwards, J. Solid State Chem. **148**, 119 (1999).

[16] M. Lemonnier, R. Fourme, F. Rosseaux, and R. Kahn, Nucl. Instrum. Methods **152**, 173 (1978).

[17] R. A. Boie, J. Fischer, Y. Inagaki, F. C. Merritt, V. Radeka, L. C. Rogers, and D. M. Xie, Nucl. Instrum. Methods **201**, 93 (1982).

[18] L. Merrill and W. A. Bassett, Rev. Sci. Instrum. **45**, 290 (1974).

[19] G. J. Piermarini, S. Block, and J. D. Barnett, J. Appl. Phys. **44**, 5377 (1973).

[20] M. Eremets, *High-Pressure Experimental Methods* (Oxford University Press, Oxford, 1996), and references therein.

[21] R. L. Snyder, in *The Rietveld Method*, edited by R. A. Young (Oxford University Press, Oxford, 1996).

[22] F. D. Murnaghan, Proc. Natl. Acad. Sci. U.S.A. **30**, 244 (1944).

[23] R. G. Munro, S. Block, and G. J. Piermarini, J. Appl. Phys. **56**, 2174 (1984).

[24] W. H. Press, B. P. Flannery, S. A. Teukolsky, and W. T. Vetterling, *Numerical Recipes: The Art of Scientific Computing* (Cambridge University Press, Cambridge, 1986).

[25] J. H. Eggert, J. Z. Hu, H. K. Mao, L. Beauvais, R. L. Meng, and C. W. Chu, Phys. Rev. B **49**, 15 299 (1994).

[26] C. C. Kim, E. F. Skelton, S. B. Qadri, V. M. Browning, M. S. Osofsky, M. E. Reeves, and D. H. Liebenberg, Phys. Rev. B **49**, 13 075 (1994).

[27] V. L. Akensov, A. M. Balagurov, B. N. Savenko, D. V. Sheptyakov, V. P. Glazkov, V. A. Somenkov, S. Sh. Shilstein, E. V. Antipov, and S. N. Putilin, Physica C **275**, 87 (1997).

[28] B. A. Hunter, J. D. Jorgensen, J. L. Wagner, P. G. Radaelli, D. G. Hinks, H. Shaked, R. L. Hitterman, and R. B. Von Dreele, Physica C **221**, 1 (1994).

[29] A. M. Balagurov, D. V. Sheptyakov, V. L. Akensov, E. V. Antipov, S. N. Putilin, P. G. Radaelli, and M. Marezio, Phys. Rev. B **59**, 7209 (1999).

[30] J. D. Jorgensen, S. Pei, P. Lightfoot, D. G. Hinks, B. W. Veal, B. Dabrowski, A. P. Paulikas, R. Kleb, and I. D. Brown, Physica C **171**, 93 (1990).

[31] J.-E. Jorgensen, J. S. Olsen, and L. Gerward, Z. Phys. B: Condens. Matter **88**, 261 (1992).